Biophysical Journal, Volume *114*

Supplemental Information

Partitioning and Enhanced Self-Assembly of Actin in Polypeptide Coacervates

Patrick M. McCall, Samanvaya Srivastava, Sarah L. Perry, David R. Kovar, Margaret L. Gardel, and Matthew V. Tirrell

SUPPORTING MATERIAL

Partitioning and Enhanced Self-Assembly of Actin in Polypeptide Coacervates

Patrick M. McCall,[a,b,1,2] Samanvaya Srivastava,[c,d,1,3] Sarah L. Perry,[c,4] David R. Kovar,[e,f] Margaret L. Gardel,[a,b,g,5,6] and Matthew V. Tirrell[c,d,5,6]

[a]*Department of Physics,* [b]*James Franck Institute,* [c]*Institute for Molecular Engineering,* [e]*Department of Molecular Genetics and Cell Biology,* [f]*Department of Biochemistry and Molecular Biology and* [g]*Institute for Biophysical Dynamics, The University of Chicago, Chicago, IL 60637, USA*

[d]*Argonne National Laboratory, Argonne, IL 60439, USA*

Footnotes:

[1] These authors contributed equally to this work.

[2] Current address: Max Planck Institute of Molecular Cell Biology and Genetics, Pfotenhauerstraße 108, 01307 Dresden, Germany

[3] Current address: Department of Chemical and Biomolecular Engineering, University of California, Los Angeles, Los Angeles, CA 90095, USA

[4] Current address: Department of Chemical Engineering, University of Massachusetts Amherst, Amherst, MA, 01003, USA

[5] These authors contributed equally to this work.

[6] To whom correspondence may be addressed. Email: gardel@uchicago.edu, or mtirrell@uchicago.edu.

SUPPORTING MATERIAL CONTENTS:

I. SUPPLEMENTAL MATERIALS AND METHODS

I.a. Polypeptide Synthesis and Storage

The racemic polyanion poly(L,D)-glutamate sodium salt (pRE) was purchased from Alamanda Polymers Inc. This is a 50/50 random copolymer of L- and D-glatamate stereoisomers. Poly(L-lysine hydrochloride) (pLK) was purchased from Alamanda Polymers Inc. or prepared in-house via N-carboxyanhydride (NCA) polymerization and characterized using gel permeation chromatography (GPC) and ^{1}H NMR (1). See Table S1 for the source, mean degree of polymerization, molecular weight, polydispersity, for the polypeptides used in each Figure.

Stock solutions were prepared gravimetrically using MilliQ water (resistivity of 18.2 MΩ-cm, Millipore) at concentrations of either 10 or 20 mM with respect to the number of monomers (that is, the number of acid or base groups) present in solution and then adjusted to pH 7.0 using concentrated solutions of HCl and NaOH, as needed. These solutions were stored at 4 °C, and wrapped in parafilm to minimize evaporation. Unless otherwise noted, peptide concentrations are reported in terms of charge equivalents. For instance, a concentration of 5 mM pLK indicates a 5 mM concentration of lysine residues, each with an average charge equivalent of +1 at pH 7. Correspondingly, the concentration of pLK molecules is 50 μM, with each pLK molecule composed of, on average, 100 +1-charged lysine residues.

I.b. Protein Purification, Labeling, and Storage

Actin was purified from rabbit skeletal muscle acetone powder (Pel-Freez) as previously described (2). A subset of gel-filtered actin was labeled on Cys-347 with either Oregon green 488 iodoacetamide (OG), Tetramethylrhodamine-5-maleimide (TMR), or pyrenyl iodoacetamide (Invitrogen) (3–5). All actins were stored in Calcium Buffer-G (CaBG: 2 mM Tris-HCl, pH 8.0 at 22 °C, 0.2 mM ATP (adenosine triphosphate), 0.5 mM DTT (1,4-Dithiothreitol), 0.1 mM $CaCl_2$, 1 mM NaN_3). Unlabeled, OG- and pyrene-labeled actins were stored at 4 °C, while TMR-labeled actin was flash-frozen with liquid nitrogen and stored at -80 °C. Prior to use, non-frozen actins were dialyzed against 0.2 L fresh CaBG for 18-24 h, and clarified via ultracentrifugation at 177,000 x g (average relative centrifugal force) for 30 minutes at 4 °C. The top 90% of the supernatant was retained, stored on ice, and used within 6 days. TMR-actin was rapidly thawed by hand, and similarly clarified via ultracentrifugation at 177,000 x g for 30 minutes at 4 °C. The top 75% of the supernatant was retained, stored on ice, and used within 2 days.

Bovine Serum Albumin (BSA) (Fraction V, Fisher Scientific) was labeled on exposed cysteines with Alexa Fluor 647 Maleimide (Invitrogen) according to the manufacturer's protocol, and stored in 1x Phosphate-Buffered Saline (PBS, pH 7.5 at room temperature) at -80 °C. Prior to use, labeled BSA was thawed rapidly by hand, and clarified by centrifugation at 21,000 x g for 20 minutes at 4 °C. The entire supernatant was retained, stored at 4 °C, and used within one month.

I.c. Protein Concentration Determination

Protein concentrations were determined spectrophotometrically. Absorbance measurements were made using an Ultrospec 2100 pro (Amersham Biosciences) or a NanoDrop ND-1000 (Thermo Scientific) UV/VIS Spectrophotometer with optical path lengths b = 1 cm and b = 0.1 cm, respectively. Sample absorbance was converted to protein concentration (and corrected for label absorbance, as appropriate) using the following expressions:

[Unlabeled-actin] = $\langle A_{290} \rangle$ *(38.5 µM cm) / b (6)

For OG-labeled actin (5):

[Total actin] = ($\langle A_{290} \rangle$ - (0.17*$\langle A_{491} \rangle$))*(38.5 µM cm) / b

[OG-actin] = $\langle A_{491} \rangle$ / ((0.0778 μM^{-1} cm^{-1})*b)

For TMR-labeled actin:

[Total actin] = ($\langle A_{290} \rangle$ - (0.1185* $\langle A_{557} \rangle$))*(38.5 µM cm) / b

[TMR-actin] = $\langle A_{557} \rangle$ / ((0.1009 μM^{-1} cm^{-1})*b)

For Pyrene-labeled actin (6):

[Total actin] = ($\langle A_{290} \rangle$ - (0.127*$\langle A_{344} \rangle$))*(38.5 µM cm) / b

[Pyrene-actin] = $\langle A_{344} \rangle$*(45.0 µM cm) / b

For BSA, the molar extinction coefficient was estimated to be E_{280} = 40,800 M^{-1} cm^{-1} using the online tool ProtParam (http://web.expasy.org/protparam/), the amino acid sequence associated with the UniProt ID P02769 for *Bos taurus* serum albumin, and assuming reduced Cys residues. The approximate extinction coefficient for Alexa Fluor 647 C_2 maleimide is E_{650} = 265,000 M^{-1} cm^{-1} (7). The concentration of BSA and Alexa Fluor 647 were thus calculated according to:

[Total BSA] = ($\langle A_{280} \rangle$ -(0.03*$\langle A_{651} \rangle$)) / ((0.0408 μM^{-1} cm^{-1})*b)

[Alexa 647] = $\langle A_{651} \rangle$ / ((0.265 μM^{-1} cm^{-1})*b)

I.d. Sample Preparation

Mg-ATP-actin is prepared in Tube A from Ca-ATP-actin by 2-minute incubation at room temperature (RT) with 1/10th volume 10x Magnesium Exchange buffer (1x ME buffer: 50 µM $MgCl_2$, 200 µM EGTA (ethylene glycol-bis(beta-aminoethyl ether)-N,N,N',N'-tetraacetic acid) in MilliQ-purified water, stored at RT). Mg-ATP-actin is then incubated at RT with either Latrunculin A dissolved in DMSO (dimethyl sulfoxide) for 5 min or an equivalent volume of DMSO, as a blank, for minimal time (< 30 s), followed by addition of pLK (or a blank of MilliQ-purified water) and incubation for 2-3 min at RT. Tube B is assembled from 10x KMEI buffer (1x KMEI: 50 mM KCl, 1 mM $MgCl_2$, 1 mM EGTA, 10 mM Imidazole, pH 7.0, stored at RT), Magnesium Buffer-G (MgBG: 2 mM Tris-HCl, pH 8.0, 22 °C, 0.2 mM ATP, 0.5 mM DTT, 0.1 mM $MgCl_2$, 1 mM NaN_3, stored on ice), and pRE (or a blank of MilliQ-purified water). Polyelectrolyte phase separation and actin polymerization is then initiated simultaneously through the addition of Tube B to Tube A and rapid mixing by pipette. Samples with ~ 1 mM or more total polypeptide are visibly turbid < 2 s after addition of Tube B to Tube A.

I.e. Microscopy

Samples were loaded into flow cells constructed from mPEG-Silane-treated glass and double-sided tape, as described previously (8). Samples were imaged at room temperature (~24 °C) on an inverted microscope (Ti-Eclipse; Nikon, Melville, NY) equipped with a confocal scan head (CSU-X, Yokogawa Electric, Musashino, Tokyo, Japan), a laser merge module (LMM5, Spectral Applied Research, Richmond Hill, Ontario, Canada) containing 488-nm, 560-nm, and 635-nm laser lines for fluorescence imaging, as well as polarizers, Nemarski prisms, and a white transmitted-light source for differential interference contrast (DIC) imaging. A 405-nm laser line was used as an excitation source for photobleaching experiments. The location of the bleached region was controlled with a micromirror array (MOSAIC, Photonics Instruments). Images were formed using a 60x, DIC-compatible, water-immersion objective (Nikon, Melville, NY) with a numerical aperature (NA) of 1.2, and corrections for apochromatic and flat field aberrations (Plan Apo). Images were acquired on a scientific complementary metal-oxide-semiconductor (sCMOS) camera (Zyla 4.2; Andor Technologies, Belfast, Northern Ireland), with a physical pixel size of 6.5 microns per side. All imaging hardware was controlled using METAMORPH acquisition software (Molecular Devices, Eugene, OR).

I.f. Image Analysis

All quantitative image analysis was performed using imageJ (NIH, imagej.nih.gov/ij/) and custom code written in MATLAB (MathWorks, Natick, MA). Camera dark noise (100 counts) was subtracted from all fluorescence images prior to analysis.

I.f.1. Measurement of average relative accumulated mass (RAM) in Figure 1E, S3, and S4. Following camera noise subtraction, fluorescence images were corrected for uneven illumination (9) using a reference fluorescence image of a plastic slide. Two masks were created for each corrected fluorescence image by thresholding. The first is called the background mask, and the second is called the droplet mask. Note that in order to reduce the impact of imaging artifacts which result from spinning-disk confocal imaging, such as pin-hole crosstalk, the background mask is not simply the inverse of the droplet mask (10, 11). We used the modal pixel intensity from the illumination-corrected fluorescence image as the threshold for the background mask. After application of the threshold, the close, invert, close, and fill holes operations were applied in ImageJ. This procedure yields a mask which excludes droplets, as well as regions outside of droplets where systematic pin-hole cross-talk effects are visible.

To create the droplet mask, the illumination-corrected image was thresholded again, this time using the average full-width-at-half-max intensity obtained from line scans across 5-10 coacervate droplets in the field of view. After application of the threshold, the invert, close, fill holes, and invert operations were applied in ImageJ.

Individual candidate droplets were then automatically identified from the droplet mask using custom code written in MATLAB. Candidate droplets were filtered by size and eccentricity. As a result of the strong peripheral localization of actin fluorescence, candidate droplets occasionally had a crescent-like morphology, similar to an unclosed circle. This occurred if the fluorescence

at some position along the droplet boundary was below the masking threshold. To remove droplets for which the mask gave unclosed circles, candidate droplets in actin fluorescence images were further filtered by removing candidates for which the center of mass fell outside the candidate droplet region. The size and average intensity of each filtered droplet was then computed using the droplet mask and the illumination-corrected fluorescence image. The average background intensity was computed using the background mask and the illumination-corrected image. Finally, the average partition coefficient for each droplet was calculated as the ratio of the average intensity within the droplet mask to the average background intensity.

I.f.2. Measurement of peripheral and interior Relative Accumulated Mass values in Figure 4E. Fluorescence intensity line scans are calculated using a transverse width of 5 pixels along paths indicated in the accompanying image, and normalized according to

$$I_{\mathrm{norm}}(x) = \left(I(x) - I_{\mathrm{min}}\right) / \left(I_{\mathrm{max}} - I_{\mathrm{min}}\right) \quad (1)$$

where *I(x)* is the intensity at position *x* along the path, and I_{min} and I_{max} are the minimum and maximum values of the intensity along the path, respectively. Interior, Periphery, and Exterior fluorescence values (e.g. Fig. 4F) are obtained from individual line scans. Interior is the average of a 5-pixel segment along the line scan, co-centered with the droplet. Periphery is the average of the maximum intensity along the line scan from either side of the droplet center. Exterior signal is calculated on each side of the droplet as the average intensity along the 6-pixel segment of the line scan extending from 10 pixels beyond the periphery peak to 15 pixels beyond the peak. The reported Exterior value is the average of the Exterior signals from each side of the line scan. One-sided Exterior values (as opposed to the average of both sides) are reported when the relevant segment on one side of the line scan impinges upon an adjacent droplet. Line scan orientation is chosen to minimize the frequency of this. These auxiliary RAM values are calculated as the ratio of either Periphery or Interior fluorescence to Exterior fluorescence.

I.f.3. Measurement of fluorescence intensity correlation coefficients. Calculation of fluorescence intensity correlation coefficients is restricted to include only pixels within droplets using a mask for each field of view. Masks were generated in ImageJ from DIC images taken at the approximate midplane of the droplet of interest by application of a Gaussian blur (radius 1.00), threshold-based conversion to a binary image, and the sequential application of the binary operations close, fill holes, and dilate, where dilate is applied twice. The intensities in the fluorescence cross-correlation histogram (e.g. Fig. 2C) are normalized independently in each channel according to equation (1) above, where the domain of *x* is all pixels identified from the mask as within droplets.

I.f.4. Measurement of fluorescence recovery after photobleaching (FRAP)

Following acquisition of pre-bleach images, photobleaching was performed by illuminating a rectangular region of interest (ROI) encompassing one or more coacervate droplets with a 405-nm laser for 5 seconds using a MOSAIC micromirror array. Camera dark noise (100 counts) was subtracted from all fluorescence images prior to analysis. The average fluorescence intensity of the bleached region is normalized according to:

$$\tilde{I}_{\text{spot}}(t) = \frac{I_{\text{spot}}(t) - I_{\text{spot}}(t_{bleach})}{I_{\text{spot}}(t_0) - I_{\text{spot}}(t_{bleach})} \quad (2)$$

where t_{bleach} is the first post-bleach frame, t_0 is the first frame acquired, and $I(t)$ is the average fluorescence intensity of the bleached region following subtraction of camera noise.

Additional, unwanted photobleaching inevitably occurs during fluorescence imaging. The timecourse of this bleaching is approximated by the decay of the fractional average fluorescence of a control droplet of the same size at time t:

$$f_{Photobleaching} = \frac{I_{\text{control}}(t)}{I_{\text{control}}(t_0)} \quad (3)$$

Note that $f_{Photobleaching}$ is unity at t_0, and decays monotonically to between 0.6 and 0.7 over 4 minutes. To account for this imaging-derived photobleaching, the normalized intensity (2) is divided by the fractional average fluorescence remaining:

$$\tilde{I}_{\text{spot,PBC}}(t) = \frac{\tilde{I}_{\text{spot}}(t)}{f_{Photobleaching}} \ . \quad (4)$$

It is this photobleach-corrected, normalized spot intensity, $\tilde{I}_{\text{spot,PBC}}(t)$, that is plotted as the FRAP recovery in Fig. S5.

I.g. Fluorescence Spectroscopy

A stock solution of 15 µM Ca-ATP-actin (typically 10-20 % pyrene-labeled) is prepared from solutions of unlabeled and highly-labeled (typically > 90 %) actin in a 1.5-mL microcentrifuge tube, and then converted from Ca-ATP-actin by 2-minute incubation with 1/10th volume 10x ME buffer and 1/10th volume of 100x anti-foam (Antifoam 204, Sigma) at RT. Mg-ATP-actin is then incubated with the desired concentration of pLK (or a blank of MilliQ-purified water) for 2-3 min at RT in up to 12 rows of a 96-well plate (Assay Plate 3686, Corning). A multichannel pipette is then used to simultaneously deliver solution assembled from 10x KMEI buffer MgBG, and pRE (or a blank of MilliQ-purified water) to the wells containing actin, thereby initiating assembly (through the addition of $MgCl_2$ and KCl) and phase separation (through the addition of the polyanion) simultaneously. The final reaction volume is 150 µL. Actin assembly is monitored at RT by pyrene fluorescence (Excitation: 365 nm, Emission: 407 nm) in a fluorescence plate reader (Saphire2, Tecan). The timecourse of pyrene excimer fluorescence (Excitation: 343 nm, Emission: 478 nm (12) was monitored concomitantly with assembly by sequentially alternating the excitation/emission wavelength pairs on a fluorescence plate reader (Infiniti m200, Tecan). We report the reciprocal of the time to 50 %-assembly ($1/t_{1/2}$) as a measure of the mean assembly rate. $t_{1/2}$ is determined for each 407-nm fluorescence timecourse as the time-point at which the fluorescence intensity is closest to $I_{1/2}$, which is defined as

$$I_{1/2} = \left(I_{\max} + I_0\right)/2 \quad (5)$$

where I_{max} is the maximum intensity of the timecourse, and I_0 is the initial fluorescence value of the actin-only control sample, which is an estimate of the sum of background contributions from the detector, buffers, and pyrene-actin monomers for all conditions.

I.h. Physical Estimates

I.h.1. Estimation of osmotic pressure required to crowd F-actin to an interface. We estimate the minimum osmotic pressure needed to crowd F-actin to an interface as that of a 0.25 % (w/v) methylcellulose solution, which is known to be sufficient (13). Using the van 't Hoff formula $\Pi = cN_A k_B T$ for the osmotic pressure of a dilute polymer at molar concentration c, where N_A is Avagadro's number, we find that a concentration of $c = 0.25\% \cong 180\ \mu M$ of 14-kDa methylcellulose gives a pressure of $\Pi^* \cong 450$ Pa at room temperature.

I.h.2. Estimation of polypeptide species concentration in dilute phase. The dilute phase concentration of a polypeptide is the critical concentration for phase separation at that temperature and salt concentration. Thus, observation of droplet formation upon mixing of pLK with pRE, each at a final global concentration X, indicates that X is greater than the critical concentration, and thereby greater than the dilute phase concentration. pLK/pRE coacervate droplets are visible by DIC at concentrations of 30 μM per polypeptide and above. However, punctate BSA fluorescence is observed at 3 μM per polypeptide, even though droplets are not readily discernible by DIC. This suggests that phase separation does still occur at this concentration. We thus use 3000 nM / 100 residues per polypeptide = 30 nM as a conservative upper bound on the dilute phase concentration for each polypeptide chain species.

I.h.3. Estimation of polypeptide concentration in coacervate phase. From dimensional analysis, we estimate the polypeptide concentration in the coacervate phase from the mass fraction according to $c = \rho_{pp} f_{pp} / M_W$, where ρ_{pp} is the mass density of a solid polypeptide substance, f_{pp} is the polypeptide mass fraction in the coacervate phase, and M_W is the polypeptide molecular weight. We estimate the polypeptide mass density ρ_{pp} as the density of solid glutamic acid, ρ_E = 1538 mg/mL (14). Unpublished measurements of f_{pp} for pLK/pRE coacervates under similar conditions find a total polypeptide mass fraction of 0.38, or 0.19 per polypeptide species. This is comparable to previously published reports on other coacervate systems, where the water content was reported to saturate at ~ 60 % (15). Using these values, and approximating the molecular weight as 12.9 kDa (Table S1), yields a polypeptide chain concentration of ~2 mM per species, corresponding to a peptide concentration of ~ 2 M per species. In the main text, we thus report the pLK concentration estimate as being on the order of 1-3 M in the coacervate phase.

I.h.4. Estimation of coacervate mesh size. We estimate the mesh size as (16) $\xi = R_F \left(\Phi^*_{pp} / \Phi_{pp} \right)^{3/4}$, where R_F is the root-mean-square end-to-end distance of the polypeptide, Φ^*_{pp} is the polypeptide volume fraction at which spheres of radius R_F containing one polymer each begin to overlap, and Φ_{pp} is the polypeptide volume fraction of the coacervate phase. Treating the polypeptides as self-avoiding flexible chains in good solvent, we have that (16)

$R_F = aN^{\nu} = aN^{3/5}$, where a is the effective monomer size of the self-avoiding chain, N is the number of such monomers per chain, and ν is the Flory exponent. We also have that $\Phi^*_{pp} \cong c^* a^3 = \frac{N}{R_F{}^3} a^3 = N^{-4/5}$, where c^* is the overlap polymer concentration. Combining these expressions gives (16) $\xi = a\Phi_{pp}{}^{-3/4}$.

We take the effective monomer size of a polypeptide in the coacervate phase to be the Kuhn length, which we estimate as (17) 0.8 +/- 0.1 nm. We estimate the volume fraction as

$$\Phi_{pp} = \frac{f_{pp}}{f_{pp} + \left(1 - f_{pp}\right)\frac{\rho_{pp}}{\rho_{\text{solvent}}}}. \quad (6)$$

Taking the total polypeptide mass fraction to be f_{pp} = 0.38 as above, and approximating ρ_{solvent} as 1000 mg/mL, we estimate the volume fraction as Φ_{pp} = 0.28. Combined with the Kuhn length estimate, this gives a mesh size estimate of ~2.1 nm. In the main text, we estimate the mesh-size as 2-3 nm in the coacervate phase.

I.h.5. Estimation of polyelectrolyte flexibility in coacervate phase. For polyelectrolytes, the total persistence length l_T can be defined by the sum of a backbone or "bare" persistence length, l_0, which derives from the chemical structure of the chain, and an electrostatic persistence length, l_E, determined by electrostatic interactions, yielding $l_T = l_0 + l_E$ (18). For the backbone persistence length, there is some uncertainty in estimating valued for pLK and pRE from the literature. Single-molecule force spectroscopy measurements of Ig-repeats from the protein titin found $l_0 = 3.9 \pm 0.1$ Å by fitting force extension curves to a worm-like chain model (19). Depending on model assumptions, analytic and numerical calculations for polyglycine give persistence lengths between 3.18 and 4.47 Å (17). We chose a value of 3.9 Å to match experiments for titin Ig domains, and which is within 20% of both the largest and the smallest model bounds.

The electrostatic persistence length can be defined as (18)

$$l_E = \frac{l_B f^2}{4\kappa^2 b^2}, \quad (7)$$

where l_B is the Bjerrum length, f is the fraction of monomers that have a charge on them, and b is the bond length of the polyelectrolyte. κ is the inverse of the Debye length, given by

$$\kappa^2 = 4\pi l_B \left[Z_c^2 c_c + \sum_\gamma Z_\gamma^2 c_\gamma \right], \quad (8)$$

where Z is the valency, c is the concentration of the ions present in the solution, and the subscripts c and γ correspond to the counterion associated with the polyelectrolyte and all the ion species contributed by the addition of salt, respectively. Combining Equations (7-8) gives

$$l_E = \frac{f^2}{16\pi \left[Z_c^2 c_c + \sum_\gamma Z_\gamma^2 c_\gamma \right] b^2}. \quad (9)$$

The electrostatic contribution is maximal in the dilute limit, where charged monomers primarily interact with and repel adjacent monomers, and in absence of added salts, which would screen electrostatic interactions. We therefore estimate the maximum persistence length for a fully charged polypeptide chain (*f = 1*) in this limit, where the sum over gamma vanishes. For a polypeptide, the bond length can be estimated as $b = 3.65\,\text{Å}$ (17). Plugging these values into Equation (9), and noting that 1 mol / L = 10^{-27} mol / Å^3, yields

$$l_E = \frac{1}{16\pi} \cdot \frac{10^{27}\,\text{Å}^3}{c_c N_A\ \text{mol}} \cdot \frac{1}{\left(3.65\,\text{Å}\right)^2} \cong \frac{2.48}{c_m}\,\text{Å}, \tag{10}$$

where c_c=c_m is the polyelectrolyte monomer concentration in units of mol / L.

Thus, in the absence of added salt in the medium (beyond counterions), we estimate the maximum persistence length of our polypeptide chains as $l_T = (2.48/c_m + 3.9)$ Å. In our pLK/pRE coacervates, we estimate $c_m \approx 2$ mol/L for each species (calculation is given above), and hence l_T = 5.14 Å. In the coacervate, however, the charge is strongly screened by both the residues from oppositely-charged chains (also at $c_m \approx 2$ mol/L) and ≈ 140 mM salt. Therefore, we expect the contribution from the electrostatic persistence length to be negligible, and the total persistence length to be essentially that of the intrinsic backbone persistence length. Therefore, we have used l_T = 0.4 nm and $b = 2l_T$ = 0.8 nm in our estimates in the manuscript.

Importantly, however, we note that the osmotic pressure required to crowd actin to a surface with a dilute solution of methylcellulose (estimated above as ≈ 450 Pa) is 3 orders of magnitude smaller than the osmotic pressure we estimate for the polypeptides in the coacervate. In terms of mesh size, the threshold for crowding is 20 nm, about an order of magnitude larger than the mesh size of 2.1 nm we quote in the section above. The mesh size is linear in the persistence length, so an order of magnitude error in the persistence length is necessary for the osmotic pressure of the pLK/pRE chains to fall below the crowding threshold. From our data, the electrostatic contribution to the polyelectrolyte rigidity is insufficient to account for this; using our lower bound monomer concentration c_m= 1 mol/L and still neglecting salt in order to maximize the persistence length only increases the mesh size to 5.8 nm.

I.i. Supporting References:

1. Kramer, J.R., and T.J. Deming. 2010. General Method for Purification of α-Amino acid-N-carboxyanhydrides Using Flash Chromatography. Biomacromolecules. 11: 3668–3672.

2. Spudich, J.A., and S. Watt. 1971. The Regulation of Rabbit Skeletal Muscle Contraction I. BIOCHEMICAL STUDIES OF THE INTERACTION OF THE TROPOMYOSIN-TROPONIN COMPLEX WITH ACTIN AND THE PROTEOLYTIC FRAGMENTS OF MYOSIN. J. Biol. Chem. 246: 4866–4871.

3. Kovar, D.R., J.R. Kuhn, A.L. Tichy, and T.D. Pollard. 2003. The fission yeast cytokinesis formin Cdc12p is a barbed end actin filament capping protein gated by profilin. J. Cell Biol. 161: 875–887.

4. Kudryashov, D.S., and E. Reisler. 2003. Solution Properties of Tetramethylrhodamine-Modified G-Actin. Biophys. J. 85: 2466–2475.

5. Kuhn, J.R., and T.D. Pollard. 2005. Real-Time Measurements of Actin Filament Polymerization by Total Internal Reflection Fluorescence Microscopy. Biophys. J. 88: 1387–1402.

6. Hansen, S., J.B. Zuchero, and R.D. Mullins. 2013. Cytoplasmic Actin: Purification and Single Molecule Assembly Assays. In: Coutts AS, editor. Adhesion Protein Protocols. Humana Press. pp. 145–170.

7. Molecular Probes. The Molecular Probes Handbook. Available at: https://www.thermofisher.com/us/en/home/references/molecular-probes-the-handbook.html [Accessed April 21, 2017].

8. Winkelman, J.D., C.G. Bilancia, M. Peifer, and D.R. Kovar. 2014. Ena/VASP Enabled is a highly processive actin polymerase tailored to self-assemble parallel-bundled F-actin networks with Fascin. Proc. Natl. Acad. Sci. 111: 4121–4126.

9. Jönsson, P., M.P. Jonsson, J.O. Tegenfeldt, and F. Höök. 2008. A Method Improving the Accuracy of Fluorescence Recovery after Photobleaching Analysis. Biophys. J. 95: 5334–5348.

10. Banani, S.F., A.M. Rice, W.B. Peeples, Y. Lin, S. Jain, R. Parker, and M.K. Rosen. 2016. Compositional Control of Phase-Separated Cellular Bodies. Cell. 166: 651–663.

11. Shimozawa, T., K. Yamagata, T. Kondo, S. Hayashi, A. Shitamukai, D. Konno, F. Matsuzaki, J. Takayama, S. Onami, H. Nakayama, Y. Kosugi, T.M. Watanabe, K. Fujita, and Y. Mimori-Kiyosue. 2013. Improving spinning disk confocal microscopy by preventing pinhole cross-talk for intravital imaging. Proc. Natl. Acad. Sci. 110: 3399–3404.

12. Bubb, M.R., L. Govindasamy, E.G. Yarmola, S.M. Vorobiev, S.C. Almo, T. Somasundaram, M.S. Chapman, M. Agbandje-McKenna, and R. McKenna. 2002. Polylysine Induces an Antiparallel Actin Dimer That Nucleates Filament Assembly CRYSTAL STRUCTURE AT 3.5-Å RESOLUTION. J. Biol. Chem. 277: 20999–21006.

13. Murrell, M.P., and M.L. Gardel. 2012. F-actin buckling coordinates contractility and severing in a biomimetic actomyosin cortex. Proc. Natl. Acad. Sci. 109: 20820–20825.

14. Pubchem. L-glutamic acid | C5H9NO4 - PubChem. Available at: https://pubchem.ncbi.nlm.nih.gov/compound/L-glutamic_acid [Accessed May 8, 2017].

15. Spruijt, E., A.H. Westphal, J.W. Borst, M.A. Cohen Stuart, and J. van der Gucht. 2010. Binodal Compositions of Polyelectrolyte Complexes. Macromolecules. 43: 6476–6484.

16. de Gennes, P.-G. 1979. Scaling Concepts in Polymer Physics. 1st ed. Ithaca, NY: Cornell University Press.

17. Hanke, F., A. Serr, H.J. Kreuzer, and R.R. Netz. 2010. Stretching single polypeptides: The effect of rotational constraints in the backbone. EPL Europhys. Lett. 92: 53001.

18. Dobrynin, A.V. 2005. Electrostatic Persistence Length of Semiflexible and Flexible Polyelectrolytes. Macromolecules. 38: 9304–9314.

19. Carrion-Vazquez, M., A.F. Oberhauser, S.B. Fowler, P.E. Marszalek, S.E. Broedel, J. Clarke, and J.M. Fernandez. 1999. Mechanical and chemical unfolding of a single protein: A comparison. Proc. Natl. Acad. Sci. 96: 3694–3699.

II. SUPPLEMENTAL TABLE

Polypeptide	Source	Degree of Polymerization	Molecular Weight (kDa)	Polydispersity	Experiments
pLK100	purchased	100	12.8	1.004	Fig. 1, 2, 3D, 4 Fig. S1, S2, S3, S4, S5
pLK126	in-house	126	16.2	1.30	Fig. 3B-C, S6
pRE100	purchased	100	12.9	1.15	Fig. 1, 2, 3D, 4 Fig. S1, S2, S3, S4, S5
pRE98	purchased	98	12.7	1.02	Fig. 3B-C, S6

Table S1. **Summary of polypeptides used in this study.**

III. SUPPLEMENTAL FIGURES

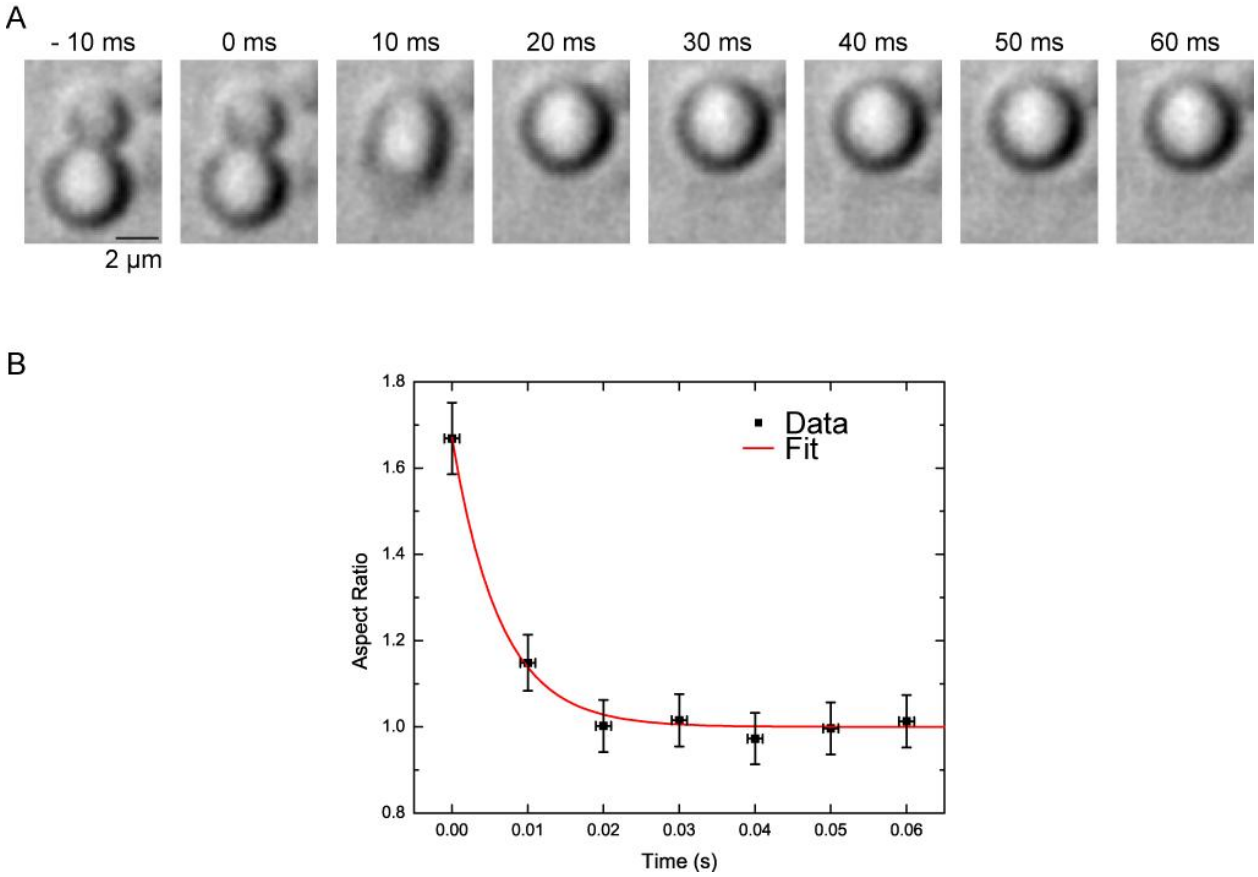

Figure S1. Liquid-like properties of pLK/pRE coacervates. (A) DIC microscopy time-lapse of two coacervates merging. Both droplets are initially round, suggestive of surface-tension dominated shapes. Upon fusing, the initially dumbbell-shaped interface rapidly relaxes to a round, surface-area-minimizing conformation of diameter d = 4 μm. (B) Aspect ratio of droplets in (A) during coalescence (black). Red line is an exponential fit, with a time constant of τ = 6.33 ms. We estimate the inverse capillary velocity as $v^{-1} = \tau/d$ = 1.6 ms/μm. Error bars represent uncertainty in aspect ratio from a single coalescence event (dy) and acquisition time (dx). Conditions are 5 mM pLK, 5 mM pRE, 50 mM KCl, 1 mM $MgCl_2$, 1 mM EGTA, 10 mM imidazole (pH 7.0), and 80 μM ATP (all concentrations final).

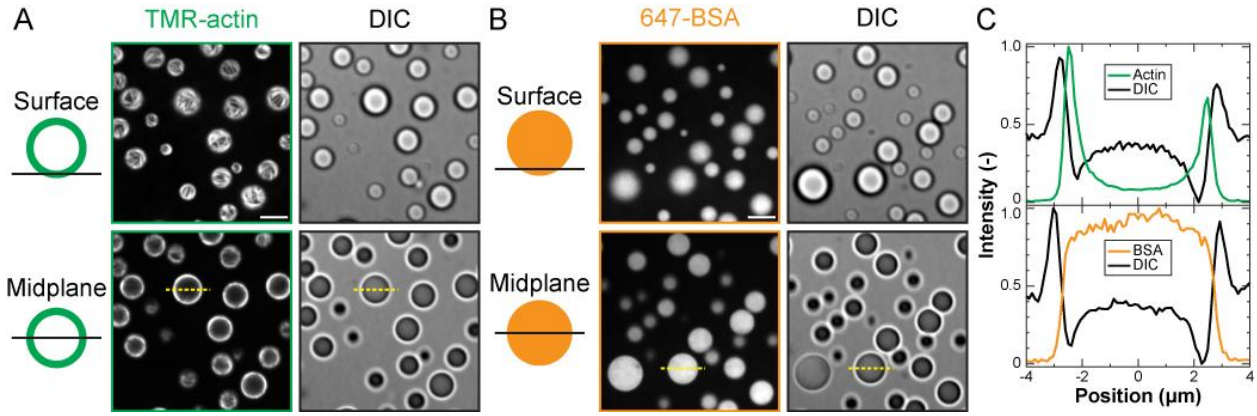

Figure S2. Peripheral localization of F-actin in polypeptide coacervates is BSA-independent. (A-B) Confocal fluorescence (left) and DIC (right) micrographs of polypeptide coacervates containing either TMR-actin (A, green) or 647-BSA (B, orange) on non-adherent substrates. Top row is focused at the interface of the coacervates and the substrate (surface), and bottom row is approximately the droplet midplane. Scale bar is 5 μm. (C) Normalized fluorescence intensity line scans along the dashed yellow lines indicated in (A) and in (B). Conditions are 0.5 μM protein (either Mg-ATP-actin (47% TMR-labeled) or BSA (91% Alexa-647-labeled)) incubated with 5 mM pLK prior to addition of 5 mM pRE in 50 mM KCl, 1 mM $MgCl_2$, 1 mM EGTA, 10 mM imidazole (pH 7.0), and 72 μM ATP (all concentrations final). Note that the average partition coefficients for (A) and (B) are reported in Figure 1 of the main text.

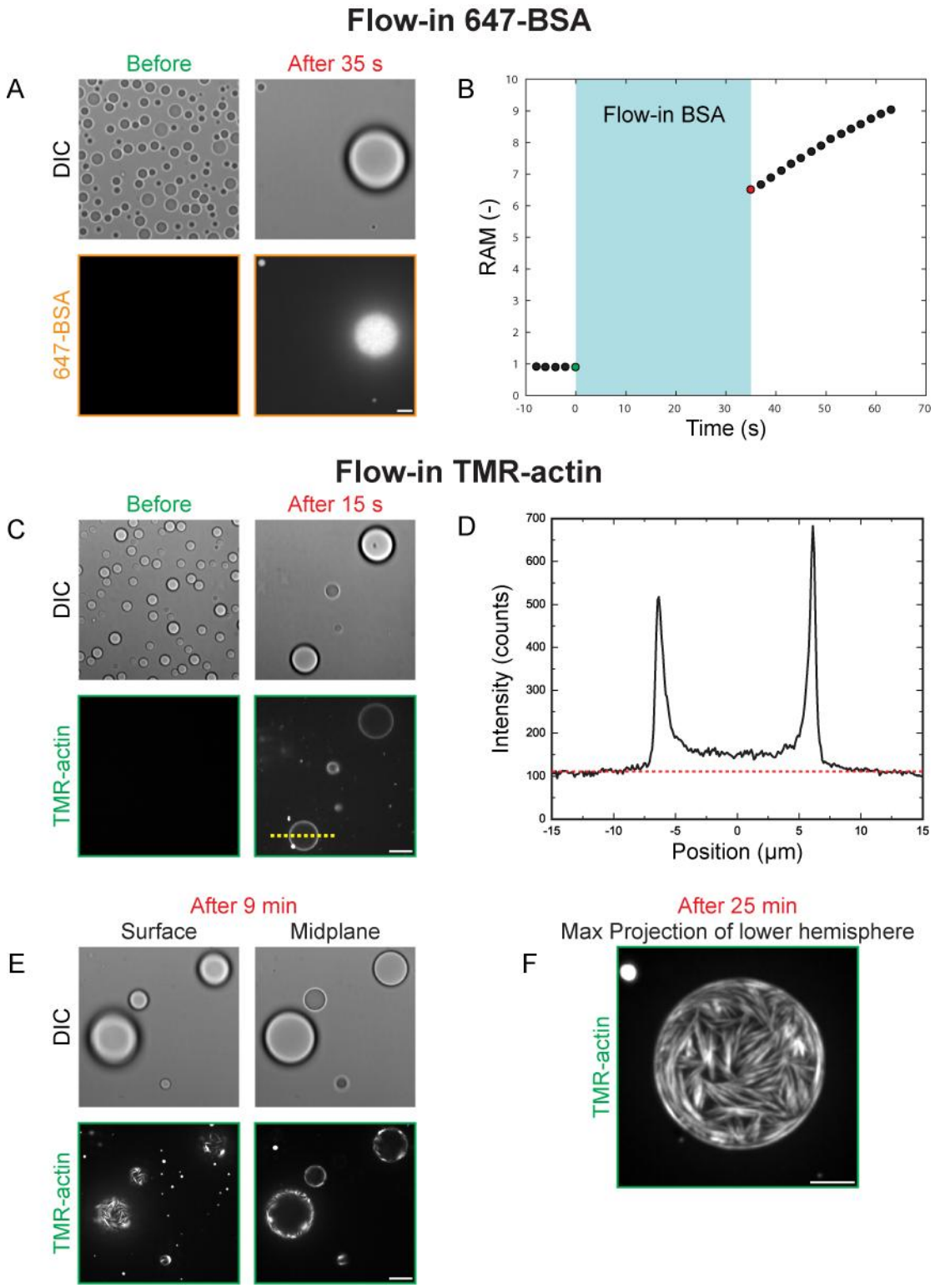

Figure S3. Flow-in of BSA or TMR-Actin to pre-formed pLK/pRE coacervates. 1.5 μM 647-BSA (A-B) or 0.25 μM TMR-actin (C-F) is perfused into a chamber containing pLK/pRE coacervates formed in the absence of protein. (A) Time-lapse confocal DIC (top) and fluorescence (bottom) micrographs of pLK/pRE coacervates before (left, green) and 35 s after (right, red) the addition of 647-BSA to the flow-cell chamber.

Figure S3. Flow-in of BSA or TMR-Actin to pre-formed pLK/pRE coacervates. (continued). Flow causes many of the sedimented droplets to fuse into larger droplets. While only background fluorescence is detectable prior to addition of BSA, BSA is partitioned to and uniformly localized within the few coacervate droplets remaining in the field of view within 35 s. Scale bar is 5 μm. (B) The RAM of the large droplet visible after BSA flow-in increases with time, but is already above 6 in the first image acquired. (C) Time-lapse confocal DIC and fluorescence micrographs before and 15 s after the addition of TMR-actin. (D) Fluorescence intensity profile along the dashed yellow line indicated in (C). The dashed red line is a guide to the eye indicating the typical fluorescence level exterior to the coacervate. Within 15 s, TMR-actin is enriched at both the periphery and interior of pLK/pRE coacervates relative to exterior levels. (E) Confocal DIC and fluorescence micrographs obtained at the coverslip surface (left) and near the coacervate midplane (right) 9 minutes following addition of TMR-actin. F-actin bundles are visible at the coacervate periphery. (F) Maximum intensity projection of confocal fluorescence micrographs obtained at 1-μm increments over an 8-μm interval. A dense network of F-actin bundles is visible. Conditions are 5 mM pLK, 5 mM pRE, 50 mM KCl, 1 mM $MgCl_2$, 1 mM EGTA, 10 mM imidazole (pH 7.0), and 72 μM ATP (all concentrations final). Proteins are perfused into the chamber in buffer containing 50 mM KCl, 1 mM $MgCl_2$, 1 mM EGTA, 10 mM imidazole (pH 7.0), and 72 μM ATP (all concentrations final). Scale bar is 5 μm in (A) and (F); 10 μm in (C) and (E).

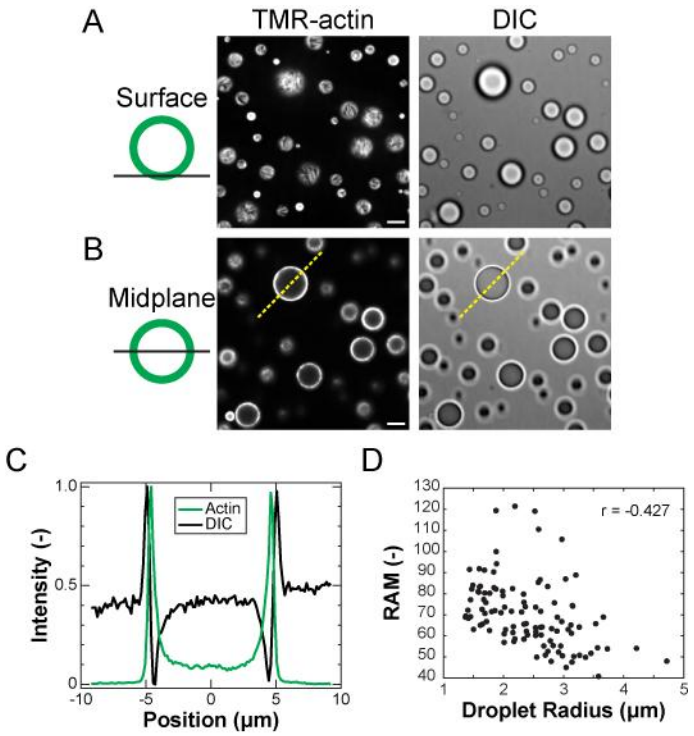

Figure S4. Partitioning and localization patterns are robust to order of addition. (A-B) Confocal fluorescence (left) and DIC (right) micrographs of polypeptide coacervates containing TMR-actin (green) on non-adherent substrates. (A) is focused at the interface of the coacervates and the substrate (surface), and (B) is approximately the droplet midplane. Scale bar is 5 μm. (C) Normalized fluorescence intensity line scans along the dashed yellow lines indicated in (B). (D) RAM of TMR-actin as a function of droplet radius, calculated for a total of N = 117 individual pLK/pRE coacervates with TMR-actin added immediately following phase separation. The average RAM is 70.3 +/- 15.9. Error bars denote the standard error of the mean. The Pearson's correlation coefficient for the data in (D) is r = -0.427, indicating a lower average partition coefficient for larger droplets. Conditions are 5 mM pLK, 5 mM pRE, 50 mM KCl, 1 mM $MgCl_2$, 1 mM EGTA, 10 mM imidazole (pH 7.0), and 72 μM ATP (all concentrations final). Following mixing and subsequent phase separation, this solution is added to a small volume of Mg-ATP-actin (47% TMR-labeled), and imaged. The final (global) concentration of actin is 0.5 μM.

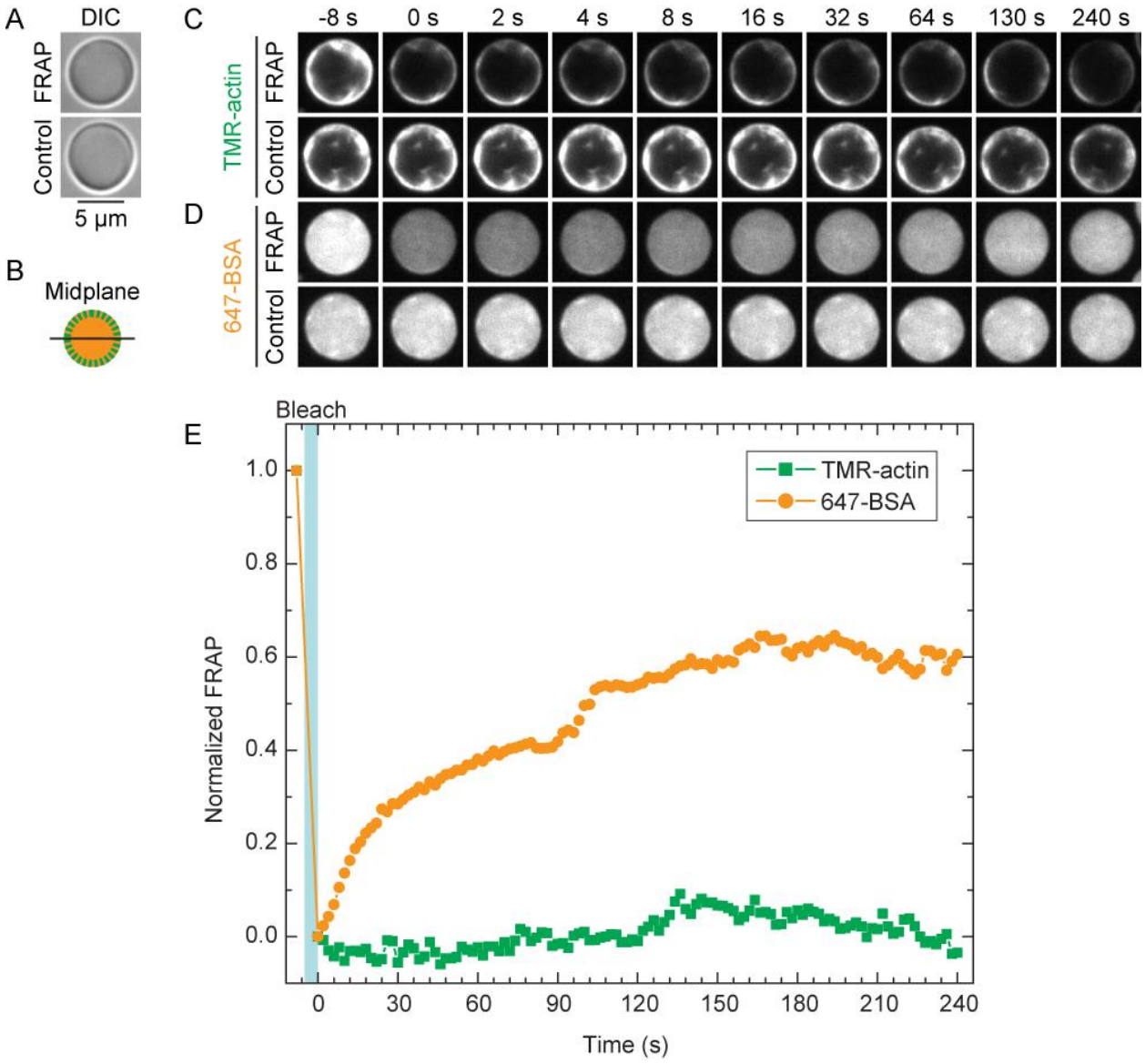

Figure S5. FRAP of partitioned actin and BSA. (A) DIC images from a single field of view of pLK/pRE coacervates into which both TMR-actin and 647-BSA are partitioned, and which are (top, FRAP) and are not (bottom, Control) subjected to a 5-second pulse of a 405-nm laser (blue shaded region in (E)). (B) Schematic denoting that images in (A) and (C-D) were acquired at the coacervate midplane. (C,D) Fluorescence images of TMR-actin (C) and 647-BSA (D) localized to coacervates which are (top rows of (C)) and (D)) and are not (bottom rows) illuminated by the bleaching laser. (E) Timecourse of the normalized average fluorescence intensity of TMR-actin (green squares) and 647-BSA (orange circles) within the coacervates shown in (C) and (D). 5-µm scale bar applies to all images. Conditions are 0.5 µM total protein (0.25 µM Mg-ATP-actin (10% TMR-labeled) and 0.25 µM BSA (91% Alexa-647-labeled)) incubated with 5 mM pLK prior to addition of 5 mM pRE in 50 mM KCl, 1 mM $MgCl_2$, 1 mM EGTA, 10 mM imidazole (pH 7.0), and 72 µM ATP (all concentrations final).

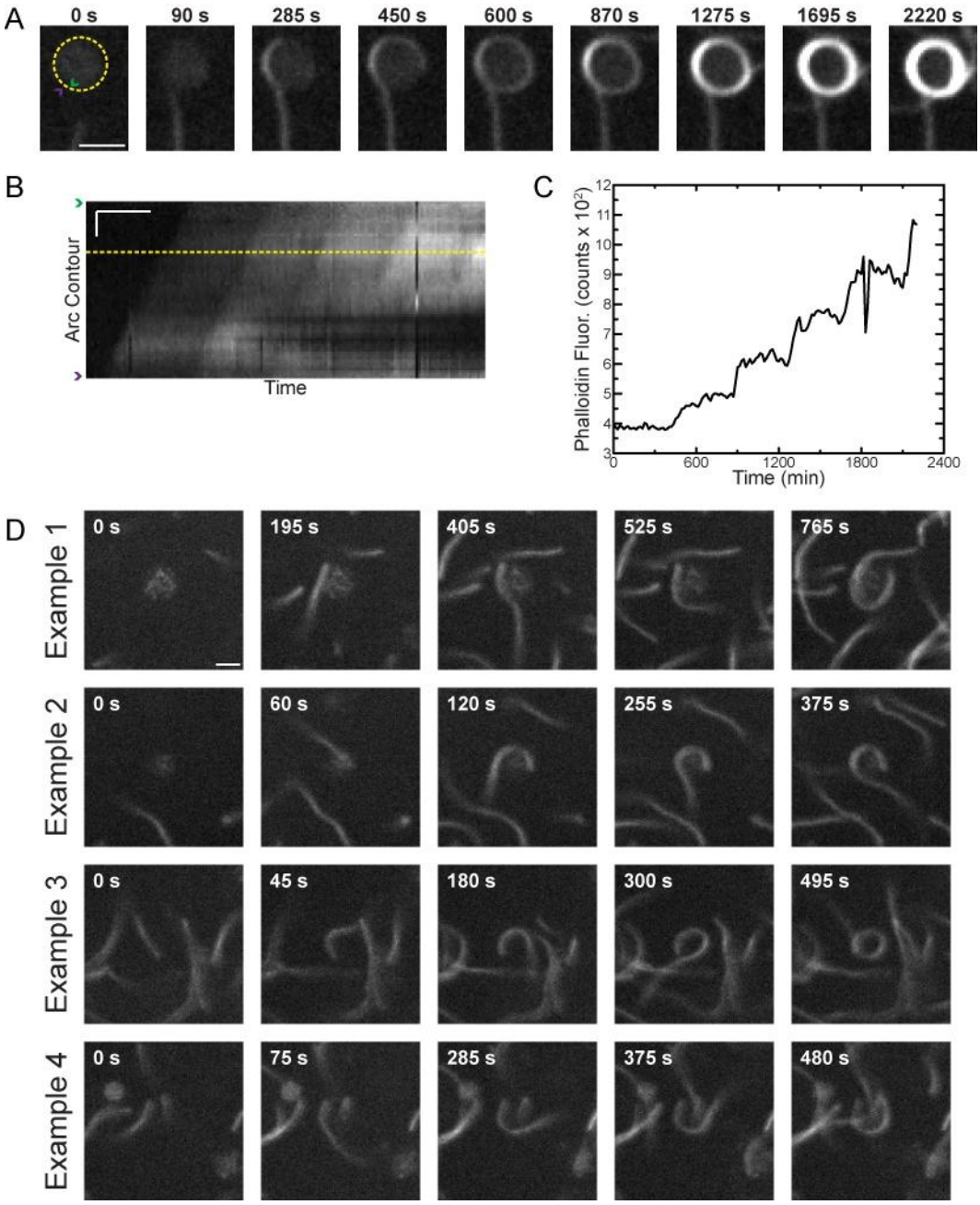

Figure S6. Adhesion of soluble F-actin to the coacervate interface. (A-D) 0.3 μM Mg-ATP-actin (unlabeled) added to a solution of 6 mM pLK/pRE coacervates and 0.2 μM Alexa488-Phalloidin in 50 mM KCl, 1 mM $MgCl_2$, 1 mM EGTA, 10 mM imidazole (pH 7.0), and 72 μM ATP (all concentrations final). (A-C) Also contain 0.5 % (w/v) 14 kDa methylcellulose (MC) and oxygen scavenging system. (A) Fluorescence time-lapse of a growing actin filament approaching a presumed coacervate droplet in presence of MC. Filament contacts coacervate, and winds around the coacervate 4 times upon further elongation. (B) Kymograph along circular yellow path in (A). (C) Intensity along yellow line scan in (B). Step-like increases indicate successive windings. (D) Examples of winding in the absence of MC. Scale bars: 2 μm (A); 1 μm and 300 s (B), 2 μm (D).

IV. SUPPLEMENTAL MOVIES

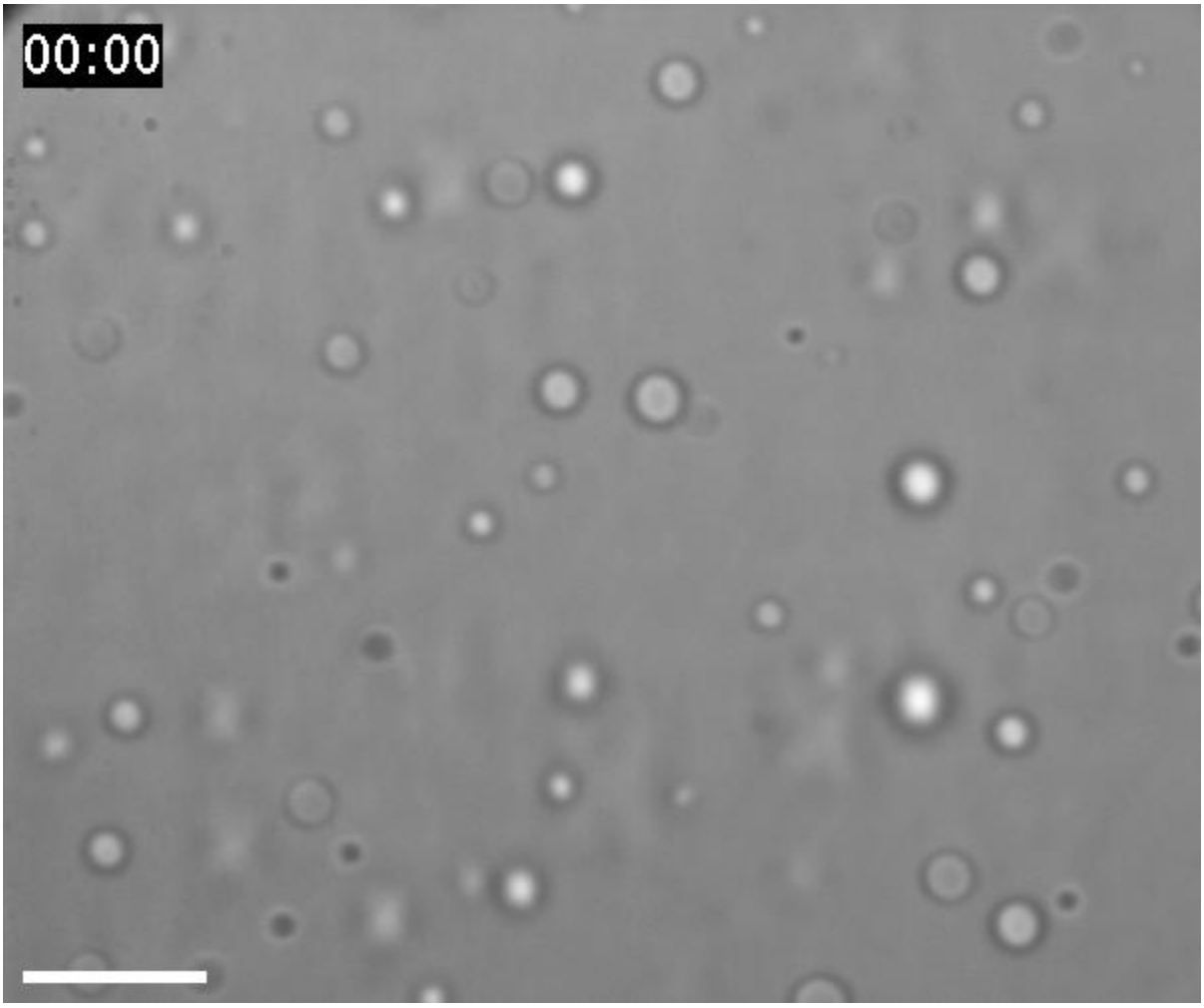

Movie S1. Coacervate droplet coalescence. Scale bar is 10 μm. Playback is 30 frames per second. Time stamp format is mm:ss. DIC timelapse imaging shows pLK/pRE coacervate droplets in solution sedimenting onto a passivated glass coverslip due to gravity. Many droplets coalescence, merging into larger droplets. Conditions are 5 mM pLK, 5 mM pRE in 50 mM KCl, 1 mM $MgCl_2$, 1 mM EGTA, 10 mM imidazole (pH 7.0), and 72 μM ATP (all concentrations final).

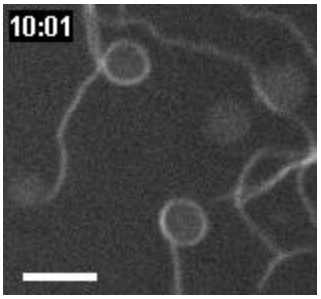

Movie S2. Adhesion of soluble F-actin to the coacervate interface. Scale bar is 4 μm. Playback is 30 frames per second. Time stamp format is mm:ss. Fluorescence time-lapse imaging shows growing actin filaments winding around presumed coacervate droplets in the presence of methylcellulose (MC). An image montage of the droplet in the lower center of the field of view is presented in Fig. S6 A. Conditions are 0.3 μM Mg-ATP-actin (unlabeled) added to a solution of 6 mM pLK/pRE coacervates and 0.2 μM Alexa488-Phalloidin in 50 mM KCl, 1 mM $MgCl_2$, 1 mM EGTA, 10 mM imidazole (pH 7.0), 72 μM ATP, 0.5 % (w/v) 14 kDa methylcellulose (MC) and an oxygen scavenging system (all concentrations final).